MATEC Web of Conferences **18**, 01004 (2014)
DOI: 10.1051/matecconf/ 20141801004

The influence of flow rate on inter-nucleation site heat transport

Coen Baltis[1] and Cees van der Geld[1,a]

[1] Department of Mechanical Engineering, Eindhoven University of Technology, P.O. Box 513, 5600 MB Eindhoven, The Netherlands

Abstract. The main topic of this paper is the influence of vertically aligned nucleation sites on each other in upward flow boiling. A setup was constructed to facilitate vertical up-flow of demineralized water under saturation conditions. The main test section is a glass channel with a set of vertically aligned bubble generators. Each bubble generator is operated independently, where power and wall temperature are registered and the vapour bubbles are visualized by a high-speed camera. During the experiments, the downstream bubble generator (BG1) power is kept constant, while the power fed to the upstream bubble generator (BG2) is incrementally increased. Two main trends have been identified. The first trend is dominated by added convection from one site to the other. Both bubble frequency and detachment diameter on BG1 increase with increased power fed to upstream BG2. This effect decreases with increasing inter-site distance and becomes more significant with increasing liquid flow rate. When vapor bubbles start nucleating from BG2, these vapor bubbles inhibit bubble nucleation BG1 and can even lead to deactivation of this nucleation site. This second trend is only weakly dependent on inter-site distance, since the inhibition originates from bubbles flowing past BG1 in close proximity.

1 Introduction

Nucleate boiling is a very efficient mode of heat transfer, yet many aspects of nucleate boiling are not well understood even today. Understanding of basic physical phenomena involved in nucleate boiling is essential to come to mechanistic models of nucleate boiling which yield realistic predictions. Note that even though such models were actively pursued (Chen (1966) [1], Stephan and Hammer (1994) [2], Steiner et al. (2004) [3], Basu et al. (2005) [4]) the predictive capacity is still poor, as shown by Kroes et al. (2009) [5] and Moghaddam and Kiger (2009) [6]. Interactions between vapour bubble nucleation sites form an important part of nucleate boiling heat transfer. In the past, many researchers studied nucleation site interactions in pool boiling, which provided better insight in the phenomenon. Unfortunately, these interactions have never before been studied in forced convection, which is the main topic of this study.

Over the past 50 years much research has been done to nucleation site interactions. Zuber (1963) [7] was one of the first to define regions of boiling with and without nucleation site interactions. Chekanov (1977) [8] was the first to study the influence of individual nucleation sites on each other in a pool boiling configuration and defining regions of influence (either promotive or inhibitive for bubble nucleation) in which the leading parameter was defined as the ratio between the mean bubble diameter, D_b, and the distance between nucleation sites, S. This ratio has been used by many researchers in the following decades (Calka and Judd (1985) [9], Kenning and Del Valle (1981) [10], Bonjour *et al.* (2000) [11], Zhang and Shoji (2003) [12]). The main consensus seems to be that nucleation site interactions are dominated by three factors of influence: 1) Hydrodynamic interactions between liquid and vapor bubbles, 2) Thermal interactions caused by conduction in the substrate, 3) Bubble coalescence. The latter has been extensively studied in more recent years (Mukherjee and Dhir (2004) [13], Siedel *et al.* (2008) [14] and Golobic *et al.* (2012) [15].

It has proven to be quite a challenge to provide reliable data with an accurate quantitative analysis. Even defining factors of influence and their importance are still up for debate. What stands out, is that all research on this subject has been performed in pool boiling. However, most cooling applications rely on forced convective heat transfer. To increase knowledge and insight in the phenomena involved in nucleation site interactions, it is therefore important to extend research to forced convective boiling. Hopefully, this will also provide a better understanding and a different perspective of the hydrodynamic interactions involved in pool boiling.

The experiments reported in this work were designed to assess the interactions between individual nucleation sites in upward saturated flow conditions.

[a] Corresponding author: c.w.m.v.d.geld@tue.nl

Article available at http://www.matec-conferences.org or http://dx.doi.org/10.1051/matecconf/20141801004

First, an overview of the experimental equipment and methods is given. Next, the main results of the experiments are described. Last, the results are analyzed and discussed, followed by the main conclusions.

2 Experiments

2.1 Test setup

A schematic of the test setup and its components can be seen in Fig. 1. During the description of the test setup below, references to the components in the schematic will be given by use of "(#)".

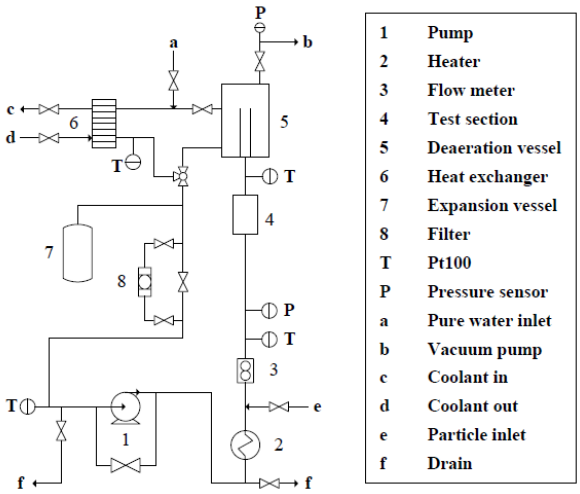

Figure 1. Schematic of the test rig

The pump (1) is a frequency controlled Grundfos CRNE 5-2 vertical centrifugal pump and is capable of delivering a maximum bulk velocity (v_{bulk}) in the test section (4) of 1 *m/s*. The pump is positioned 4 meters below the test section, which increases the local pressure by 0.4 *bar* and prevents the pump from cavitating. The flow meter (3) is positioned upstream of the test section and measures the flow using ultrasonic waves (Krohne UFM 3030). This type of measurement does not disturb the flow and causes an insignificant pressure drop, both of which are important advantages. The flow meter has an expected measurement error of 0.5% of the measured value. The upflow channel and test section have a cross section of 30x30 mm^2. To ensure fully developed flow conditions in the test section, the free flow length in front of the test section is 40 hydraulic diameters long and preceded by a tube bundle flow straightener. Furthermore, the flow meter, which is positioned before the flow straightener, has a contraction which is also known to be advantageous for flow development.

Accurate temperature control is vital for boiling experiments. In order to minimize heat losses, the complete setup has been insulated using 6 *mm* thick Armaflex. During the main experiments, this insulation was found to be sufficient since the difference in temperature between heater and test section (4 meters in length) was 0.2 *K* at maximum. The fluid is heated up by an immersion heater (2) of 17 *kW*. In order to maintain a steady fluid temperature with 0.1 *K* accuracy, a Pt100 is positioned right above the test section and connected to a Eurotherm 2408 PID controller which regulates the heater. A plate heat exchanger (6) with a maximum capacity of 30 *kW* can be utilized to cool down the liquid when desired. The orientation and placement of the heater are chosen such that any hot liquid and bubbles, as a result of degassing, will rise straight up past the test section and into the deaeration vessel (5), which seperates air bubbles from water by buoyancy. Any remaining microbubbles are captured by a Spirovent deaerator. The setup is deaerated by circulating the water at a temperature of 101 °*C* at ambient pressure for several hours.

The system pressure is monitored by a pressure transducer (P) which has an accuracy of 0.035 *bar*. To stabilize the pressure, an expansion vessel (7) with pressure control on the air-side of the vessel is employed.

2.2 Test section

The test section used during the experiments has been custom made to meet high requirements. First and foremost, the test section has to contain nucleation sites for vapour bubbles to grow. Special requirement of these nucleation sites is that the temperature of the wall can be measured. Second, clear visibility of the vapour bubbles and flow are of great importance to the accuracy of measurements. Third, any materials used in this design have to be able to withstand the system temperature range and working fluid. These requirements led tothe design presented below.

Due to the requirement of temperature measurement or temperature control of the bubble nucleation area, choice was made for 1x1 mm^2 titanium thin film resistors with a thickness of 200 *nm* as bubble nucleation sites. The advantage of such thin films is that their resistance is sensitive for temperature fluctuations, with an average positive temperature coefficient of 0.01 *Ω/K*. When the resistance changes, any current and voltage flowing through the resistor will also change. By keeping the current through this resistor constant and measuring the voltage drop, its resistance and, therefore, temperature can be determined.

The thermal response time of the thin film layer is dependent on its thermal diffusivity, α, and thickness, *L*. For a typical Fourier number (Fo) of one, the thermal response time, τ_{TF}, is

$$\tau_{TF} = \mathrm{Fo} L^2 \alpha = 5\ ns. \quad (1)$$

Therefore, the thin film resistance is a direct measure for the instantaneous wall temperature (T_{wall}).

The test section consists of a glass channel with a square cross section of 30x30 mm^2. On one wall of the channel, a grid of thin film resistors has been placed by chemical vapour deposition. By the same process, golden leads with a thickness of 500 *nm* have been deposited, which act as electric conductors. A picture of the test section can be seen in Fig. 2, along with the main bubble

generator grid and a close-up view of this grid. The vertical spacing between the top seven bubble generators is 1 *mm* and these are the main generators used in this experimental investigation. They are positioned in the horizontal center of the wall. The bottom three generators are placed horizontally, also with a spacing of 1 *mm*. These bubble generators were not used in the current investigation. An important note to make here, is that all bubble generators are connected to a common exit lead. In the next section, this exit lead will be shown to play a significant role in the determination of the bubble generator resistances.

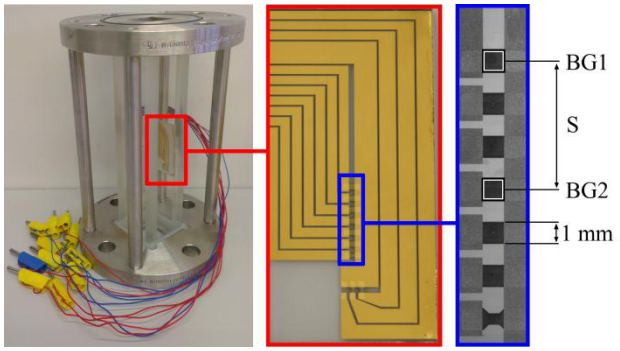

Figure 2. Left) Glass test section for bubble nucleation; Middle) Glass wall with deposited golden leads and titanium heaters; Right) Close-up of the vertically aligned bubble generator grid

2.3 Data acquisition and control

Power is fed to the bubble generators by use of constant current (CC) power sources. The voltage drop over the bubble generators is measured at 10 *kHz* sampling frequency. Use of Ohm's law then results in the resistance of the bubble generator. The electric scheme can be seen in Fig. 3.

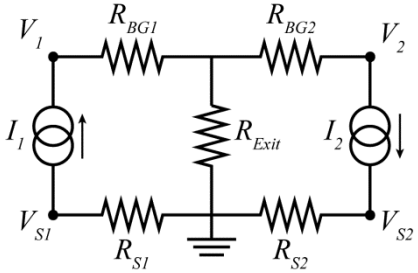

Figure 3. Electric scheme used to operate two bubble generators simultaneously

All voltages, V, in this scheme are measured with respect to the ground. Resistances R_{S1} and R_{S2} are known shunt resistances, used to determine the current, I, through the bubble generators R_{BG1} and R_{BG2}. The common exit resistance, R_{Exit}, is of significant influence on the results. Only when the resistance of the exit lead is known exactly, there is no influence of this resistance on the calculation of the resistances of BG1 and BG2. Calculation of the resistances on BG1 and BG2 is done by

$$R_{BG1} = (V_1 - V_{Exit})/I_1, \qquad (2)$$

where

$$V_{Exit} = (I_1 + I_2)R_{Exit} = \left(\frac{V_{S1}}{R_{S1}} + \frac{V_{S2}}{R_{S2}}\right) R_{Exit}, \qquad (3)$$

in which V_1, V_{S1} and V_{S2} are measured, and R_{S1} and R_{S2} are known. Assuming a constant R_{Exit} and R_{BG1}, which is valid when I_1 is constant, both resistances can be determined by varying I_2.

An analysis of errors has lead to the following conclusions. The resistance of a single active bubble generator can be determined up to 0.01 Ω precision. For two active bubble generators, there is an added error which can cause an increasing or decreasing linear trend in the resulting resistance of both bubble generators, with a maximum of 0.02 Ω. The implications for temperature determination of the bubble generators are clear. An accuracy of 0.01 Ω corresponds roughly to an accuracy of 1 *K*, which is also the accuracy of a single active bubble generator. When two bubble generators are active, the upward or downward trend corresponds to a maximum error of ±2 *K*.

Figure 4. Optical setup used during the experiments

The acquisition of the electrical data is synchronized with an optical acquisition system consisting of one cameras and two light sources, as shown in Fig. 4. The camera (Photron SA3, 5,000 *FPS*) records the top view of the nucleating bubbles. A 50 *W* PowerLED (Bridgelux) is placed directly opposite to the camera and a Dedocool, placed above the camera, is used for extra lighting on the top view. Direct shadowgraphy is impossible due to the titanium and golden layers partially blocking the light from the back.

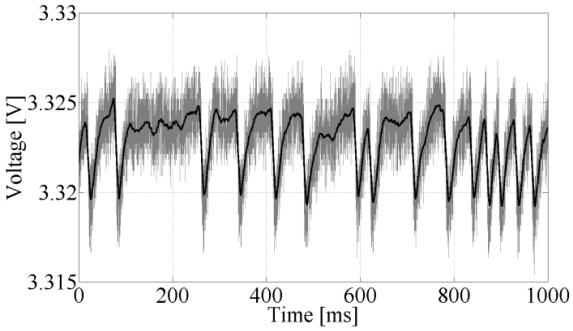

Figure 5. Voltage peaks resulting from bubble nucleation events, used to determine the bubble frequency

The first main parameter reported in the results section is the bubble frequency. The frequency is determined by analyzing the voltage drop across the bubble generator. When a bubble nucleates on a bubble generator, it draws heat from the titanium layer and the glass underneath. This effect cools down the resistor and lowers its resistance. Because the current is kept constant and the resistance decreases, the voltage must also decrease as prescribed by Ohm's law, $V = IR$. An example voltage measurement is presented in Fig. 5. The data (in grey) is smoothed using a 100-point moving average, resulting in the black graph.

In this example, a total of 15 bubbles nucleated in 1 second, each of which caused a voltage drop of around 4-5 mV. In the analysis, the derivative of the signal is taken and, in combination with a suitable threshold value, the bubble frequency is extracted from these data. In the experiments reported below, the bubble frequency was determined over a time span of 30 seconds per measurement point. In the results section, the accuracy in the frequency is given by the standard error of the mean. The frequency is the reciprocal of the average waiting time, τ_w, for which the standard error of the mean for a finite set of N samples is given by

$$s_{\overline{\tau_w}} = \sqrt{\frac{1}{N(N-1)}\sum_{i=1}^{N}(\tau_i - \overline{\tau_w})^2}. \quad (4)$$

It was found that the location of the natural nucleation site on BG1 changed between experiments. The above analysis of bubble frequency was applied to the experiments reported for the lowest flow velocity, v_{bulk} = 0.45 *m/s*, in which BG1 produced relatively large (~1.5-2 *mm*) bubbles causing a significant voltage drop. However, a different nucleation site was active on BG1 in the measurements at the higher flow velocity 0.85 *m/s*, as described in more detail in the results section. This nucleation site produced smaller bubbles and, therefore, caused less significant voltage drops, making accurate nucleation frequency determination difficult. Therefore, the nucleation frequencies for these measurements have been determined from 10 second camera recordings.

The second main parameter reported in the results section is the bubble radius. This radius is determined at detachment by taking the average of two lengths in the top view camera images, shown in Fig. 6, and dividing by two. The accuracy of sizes a and b is 1 pixel, which corresponds to 0.022 *mm*, or ca. 1% of length a or b.

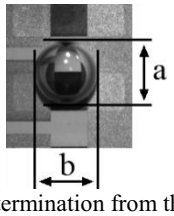

Figure 6. Size determination from the top view image

2.4 Experimental procedures

During all experiments, the bulk liquid temperature, T_{bulk}, was around 101.0 ±0.1°*C* and the local bulk pressure, p_{bulk}, at the height of bubble generator grid was 1.05 *bar*. These values meet near saturation conditions. The main objective of the experiments is to study the influence of one bubble generator on another one. Therefore, two bubble generators are activated at the same time. For all experiments presented in the results section, the power to the top bubble generator (i.e. the generator positioned highest, from here on referred to as "BG1") is kept constant. The second bubble generator, positioned upstream from BG1, is labelled "BG2". The power fed to BG2 is varied during the experiments, and is incrementally increased from 0 *W* to the point where the bubble frequency from this bubble generator is roughly 100 *Hz*. This limit was chosen because of the fragile nature of the thin films; when the layer does not get sufficient cooling, it can locally overheat and break. The second variable in the experiments is the inter-site distance, *S*, which is defined as the distance between the centers of the bubble generators. Additionally, it should be stressed that bubbles do not necessarily nucleate from the exact center of the bubble generator. The value of the inter-site distance is varied from 2 to 10 *mm*. Lastly, the bulk flow velocity, v_{bulk}, is varied in order to study the influence of this parameter on inter-site heat transport. The investigated flow velocities are 0.45 and 0.85 *m/s*.

For clarity, Fig. 7 shows schematically the side view of the situation described above. The added convective heat and nucleating bubbles from BG2 are expected to influence bubble frequency and detachment diameter at BG1.

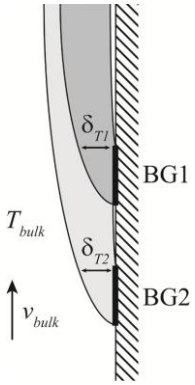

Figure 7. Influence of BG2 on BG1

3 Results

The bubble frequency response to increasing P_{BG2} for an inter-site distance, *S*, of 2 *mm* is shown in Fig. 8. As mentioned above, the power on the downstream bubble generator, BG1, is constant during the experiments, as well as all other system parameters. The wall temperature of BG1 before activation of BG2 was 112±1°*C*. The nucleation frequency increases with P_{BG2}. When the power to BG2 is large enough to initiate significant bubble nucleation at BG2 itself, the bubble frequency at BG1 starts decreasing as the frequency of BG2 increases.

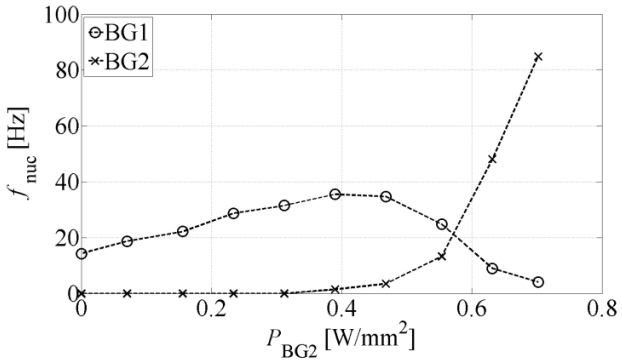

Figure 8. BG1 bubble frequency dependency on power fed to BG2 for varying inter-site distance *S*

The same experiments have been at several inter-site distances, the result of which can be seen in Fig. 9. The error bars in the figure represent the standard error of the mean, see Eq. 4. For comprehensibility of the graphs, the error bars are shown only for an inter-site distance of 6 *mm*. The value of the standard error of the mean is ~0.5 *Hz* for all experiments. One important thing to stress here, is that BG1 in this analysis is the same bubble generator, but the upstream generator is chosen further away with each step, i.e. physically different according to Fig. 2. Every bubble generator starts bubble nucleation at a different power and also bubble radius at detachment varies from 0.6 to 1.0 *mm*, for various bubble generators. The time of significant (>1 *Hz*) bubble nucleation initiation from BG2 is denoted by a filled marker.

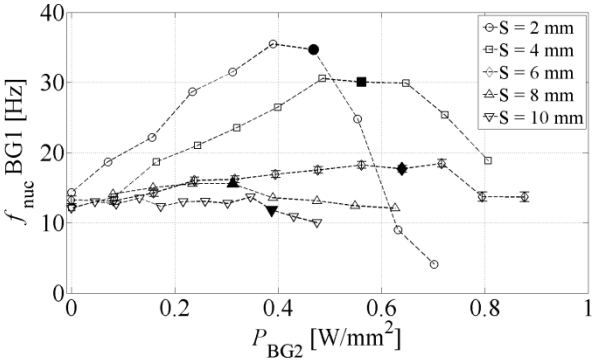

Figure 9. BG1 bubble frequency dependency on power fed to BG2 for varying inter-site distance *S*

For an inter-site distance of up to 8 *mm*, the bubble frequency of BG1 increases while BG2 is not creating its own bubbles. The most significant effect can be seen for distances of 2 and 4 *mm*. A decrease in f_{BG1} can be seen for all inter-site distances after BG2 starts creating its own bubbles (filled marker).

The relative increase of the bubble diameter, defined as the maximum bubble diameter, $D_{b,max}$, at a certain $P_{BG2,max}$ divided by the bubble diameter as observed without influence of BG2, $D_{b,0}$, is shown in table 1 for all intersite distances. The bubble radius for *S* = 2 *mm* increases by around 22%, until BG2 initiates nucleation. The detachment radius was not quantified for vapor bubbles that are influenced in their growth and detachment by bubbles originating from BG2. Because of this, the detachment radius is not shown for higher values of P_{BG2}. The increase in bubble detachment size shows similarities to the increase in bubble frequency. The most significant influence is seen in short inter-site distances of 2, 4 and 6 *mm*. For the larger distances of 8 and 10 *mm*, the detachment radius increase is relatively small.

Table 1. Increase in bubble detachment diameter for v_{bulk} = 0.45 *m/s*, the standard error of the mean is ±2% at most (95% confidence bounds)

S **[mm]**	$P_{BG2,max}$ **[W]**	$D_{b,0}$ **[mm]**	$D_{b,max}$ **[mm]**	**Increase [%]**
2	0.39	1.56	1.90	21.8
4	0.49	1.64	1.86	13.4
6	0.56	1.66	1.81	9.0
8	0.24	1.65	1.72	4.2
10	0.35	1.65	1.70	3.0

As mentioned in the section 2.3, the location of the active nucleation site on BG1 was different in the experiments performed at the higher flow rate (0.85 *m/s*). The implications of the change in nucleation site location will be further discussed in the analysis section 4.

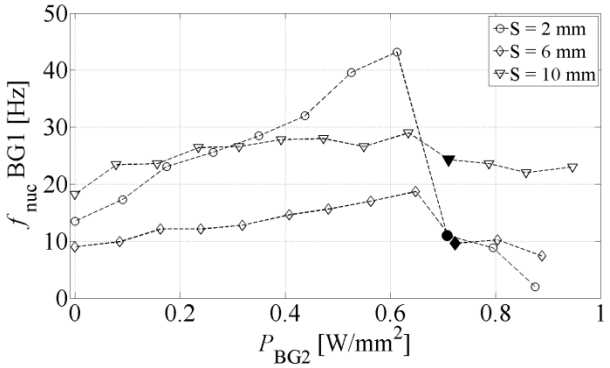

Figure 10. BG1 bubble frequency dependency on power fed to BG2 for varying inter-site distance S at v_{bulk} = 0.85 *m/s*

The experiments for v_{bulk} = 0.85 *m/s* have been performed at inter-site distances of 2, 6 and 10 *mm*. The resulting frequency histories can be seen in Fig. 10. The observed trends are similar to the ones reported for lower flow rates, see Fig. 9. Contrary to the lower flow rate is that even at a distance of 10 *mm* a significant increase in bubble frequency can be observed. Furthermore, the relative increase and decrease in bubble frequency at a distance of 2 *mm* is more severe, even leading to near complete deactivation of the nucleation site at BG1.

Table 2. Increase in bubble detachment diameter diameter for v_{bulk} = 0.85 *m/s*, the standard error of the mean is ±2% at most (95% confidence bounds)

S **[mm]**	$P_{BG2,max}$ **[W]**	$D_{b,0}$ **[mm]**	$D_{b,max}$ **[mm]**	**Increase [%]**
2	0.62	1.34	1.57	17.9
6	0.64	1.32	1.41	7.6
10	0.66	1.28	1.33	4.7

The mean bubble departure diameter for each inter-site distance and its relative increase at v_{bulk} = 0.85 *m/s* is denoted in table 2. The increase is comparable to, but slightly lower than the ones reported for v_{bulk} = 0.45 *m/s* in table 1.

4 Discussion

The increase in bubble frequency at the downstream bubble generator, BG1, with increasing P_{BG2} until significant bubble nucleation commences at BG2 (Fig. 8) is explained by the increasing convective heat added to the liquid flow by BG2. Visualization of the heat originating from the bubble generators by a side-view camera is possible due to temperature gradients near the bubble generator surface, causing changes in refractive index. Based on these recordings, a schematic representation of this situation is drawn in Fig. 7. As a consequence of the increased convective heat, the thickness of the thermal boundary layer at BG1, δ_{T1}, and the average temperature in the volume adjacent to BG1 in the boundary layer, $\overline{\Delta T}$, increase with increasing P_{BG2}. The heat convection from the upstream bubble generator promotes nucleation at the downstream site, BG1.

When BG2 starts creating vapor bubbles of its own, the bubble frequency of BG1 starts decreasing. The explanation for this is has three combined reasons:

- The added convective heat that BG1 was receiving from BG2 is suddenly lower because vapor bubbles nucleate at BG2.
- When a vapor bubble originating from the upstream bubble generator moves towards and passes by BG1, it scavenges away the heat in the thermal boundary layer of BG1 for additional evaporation which leads to an increase in size of this bubble.
- When a bubble passes by BG1, its low pressure wake will enhance mixing and will direct more hot liquid away from the surface. Convective heat transfer from BG1 is enhanced.

When increasing the inter-site distance, see Fig. 9, the added convection keeps showing a significant contribution to the promotion of bubble nucleation, but the largest effect can be seen for distances of 2 and 4 *mm*. At larger distances, the added heat is mixed into the bulk liquid flow and its contribution rapidly decreases. The inhibitive effect of bubbles passing by BG1 can be seen for every inter-site distance. Unlike the convective promotion, the inhibitive effect is present even for $S = 10$ *mm*. This effect is expected to play a role at even larger distances than reported here, but is therefore dependent on the flow direction. In the reported experiments, the flow is vertically upward with respect to gravity. The lift force on isolated bubbles originating from upstream generator BG2 acts in the direction of the wall, as shown by Tomiyama *et al.* (1998) [16], valid for Eötvös number, $Eo < 4$, corresponding to $D_b < 5$ *mm*. Therefore, the lift force moves bubbles towards the wall as they flow upward. This, in turn, means that the vapor bubbles travel at close proximity past other nucleation sites, inhibiting bubble nucleation

With respect to bubble diameter, see tables 1 and 2, the same trend is observed as for f_{BG1}. With increasing inter-site distance, the relative increase in bubble radius decreases. The influence of added convection originating from BG2 diminishes with increasing S. For $v_{bulk} = 0.45$ *m/s*, the added convection has almost no influence on the larger distances of 8 and 10 *mm* anymore, since most of the heat is diffused away into the bulk flow. From pool boiling experiments, short distance nucleation site interactions were already known to be the consequence of hydrodynamic interactions of neighboring bubbles and conduction in the substrate. This obviously affects the number of active nucleation sites. Short-distance interaction of this kind is expected to play a similar role in forced convective boiling. However, the present study has shown that hydrodynamic nucleation site interactions play a significant role at even larger distances in flow boiling. Hydrodynamic interaction is prolonged by the advection of bubbles to other nucleation sites.

Table 3. Comparison of the relative increase in bubble frequency between the two observed flow rates

S [mm]	f_{BG1} increase [%] *(0.45 m/s)*	f_{BG1} increase [%] *(0.85 m/s)*
2	157	258
6	38	90
10	8	61

When increasing the liquid bulk flow rate, the increase in bubble frequency is enhanced for all inter-site distances S, as is summarized in table 3. However, from the increase in diameter the same conclusion can not be drawn, as can be deducted from tables 1 and 2. The increase in bubble radius is comparable to the radius increase reported for $v_{bulk} = 0.45$ *m/s* and for all inter-site distances. However, in this measurement the bubble nucleation site location was different, as can be seen in Fig. 11. The location is near the left edge of the heater area and bubbles originating from this location will, for almost half the bubble width, grow over the left edge of the heater. This means that the bubble will partially grow into a colder region of liquid.

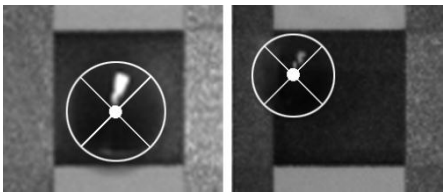

Figure 11. Natural nucleation site locations on BG1 observed during the experiments; Left) $v_{bulk} = 0.45$ *m/s*; Right) $v_{bulk} = 0.85$ *m/s*

The difference in nucleation site is therefore part of the reason why bubbles originating from this location are smaller at detachment compared to bubbles formed at $v_{bulk} = 0.45$ *m/s*. Additionally, the bulk flow velocity is higher, which means that the bubble will leave the heater area faster (see Baltis & Van der Geld (2014) [17]), also contributing to a smaller bubble detachment size. For this reason, it is not unreasonable to think that the relative increase and decrease in bubble frequency and bubble diameter would have been even more pronounced when the bubble nucleation location was still in the center of the bubble generator.

5 Conclusion

An experimental setup was constructed to perform nucleate boiling experiments in upward flow conditions, in order to investigate the influence of vertically aligned vapour bubble nucleation sites on one another. The experiments were performed by activation of two bubble generators, of which the inter-site distance can be varied with steps of 2 *mm*. Depending on mass flow rate, flow direction and heat fluxes to both bubble generators, nucleation sites have been shown to interact even at the largest observed distance of 10 *mm*, but are believed to play a role at any distance, as long as already existing vapor bubbles travel in close proximity to nucleation sites. The results have shown two major trends.

The first trend is caused by added convection from the lower bubble generator (BG2) to the upper bubble generator (BG1), as schematized in Fig. 7. The influence of additional convection on bubble frequency and diameter diminishes with increasing inter-site distance, S, and initial bubble nucleation frequency at BG1, f_{BG1}. The influence of added convective heat is shown to be enhanced by increasing the liquid bulk flow rate.

The second trend is seen when BG2 initiates bubble nucleation. Vapour bubbles that nucleate at BG2 and pass by BG1 have an inhibitive effect on bubble nucleation at BG1. The inhibitive effect does not seem to be strongly dependent on the inter-site distance, because in upward boiling flow, bubbles have been found to move towards the wall due to the lift force.

Because of the significance of the effect of hydrodynamic interaction on the number of active nucleation sites and bubble size at detachment, mechanistic modeling of nucleate flow boiling is expected to benefit from the above findings.

References

1. J.C. Chen, Ind. & Eng. Chem. **5(3)**, 322-329 (1966)
2. P. Stephan, J. Hammer, Wärme- und Stoffübertragung **30**, 119-125 (1994)
3. H. Steiner, A. Kobor, L. Gebhard, Int. J. Heat Mass Transfer **48**, 4161-4173 (2004)
4. M. Basu, G.R. Warrier, V.K. Dhir, J. Heat Transfer **127**, 131-140 (2005)
5. J.P. Kroes, C.W.M. van der Geld, E. van Velthooven, Adv. Multiph. Flow Heat Transfer **1**, 267-283 (2009)
6. S. Moghaddam, K. Kiger, Adv. Multiphase Flow Heat Transfer **1**, 267-283 (2009)
7. N. Zuber, Int. J. Heat Mass Transfer **6**, 53-78 (1963)
8. V.V. Chekanov, Teplof. Vys. Temp. **15**, 121-128 (1977)
9. A. Calka, R.L. Judd, Int. J. Heat Mass Transfer **28**, 2331-2342 (1985)
10. D.B.R. Kenning, M.V.H. del Valle, Int. J. Heat Mass Transfer **24**(6), 1025-1032 (1981)
11. J. Bonjour, M. Clausse, M. Lallemand, Exp. Thermal Fluid Sci. **20**, 180-187 (2000)
12. L. Zhang, M. Shoji, Int. J. Heat Mass Transfer **46**, 513-522 (2003)
13. A. Mukherjee, V.K. Dhir, J. Heat Transfer **126**, 1023-1039 (2004)
14. S. Siedel, S. Cioulachtjian, J. Bonjour, Exp. Thermal Fluid Sci. **32**, 1504-1511 (2008)
15. I. Golobič, J. Petkovsek, D.B.R. Kenning, Int. J. Heat Mass Transfer **55**, 1385-1402 (2012)
16. A. Tomiyama, H. Tamai, I. Zun, S. Hosokawa, Chem. Eng. Sci. **57**, 1849-1858 (2002)
17. C.H.M. Baltis, C.W.M. van der Geld, J. Fluid Mech. (2014), *submitted*